Silyl-Functionalized Electrolyte Additives and Their Reactivitytoward Lewis Bases in Li-Ion Cells br

(article starts on next page)

Silyl-Functionalized Electrolyte Additives and Their Reactivity toward Lewis Bases in Li-Ion Cells

Neeha Gogoi,* Erik Bowall, Robin Lundström, Nataliia Mozhzhukhina, Guiomar Hernández, Peter Broqvist, and Erik J. Berg*

ACCESS | Metrics & More | Article Recommendations | Supporting Information

ABSTRACT: Silyl groups are included in a wide range of electrolyte additives to enhance the performance of state-of-the-art Li-ion batteries. A recognized representative thereof is tris-(trimethylsilyl)phosphate (TMSPa) which, along with the similarly structured phosphite, has been at the center of numerous electrolyte studies. Even though the silyl group has already been widely reported to be specifically reactive towards fluorides, herein, a reactivity towards several Lewis bases typically found in Li-ion cells is postulated and investigated with the aim to establish a more simplified and generally applicable reaction mechanism thereof. Both gaseous and electrolyte soluble reactants and products are monitored by combining nuclear magnetic resonance and injection cell-coupled mass spectrometry. Experimental observations are supported by computational models. The results clearly demonstrate that the silyl groups react with water, hydroxide, and methoxide and thereby detach in a stepwise fashion from the central phosphate in TMSPa. Intermolecular interaction between TMSPa and the reactants likely facilitates dissolution and lowers the free energy of reaction. Lewis bases are well known to trigger side reactions involving both the Li-ion electrode and electrolyte. By effectively scavenging these, the silyl group can be explained to lower cell impedance and prolong the lifetime of modern Li-ion batteries.
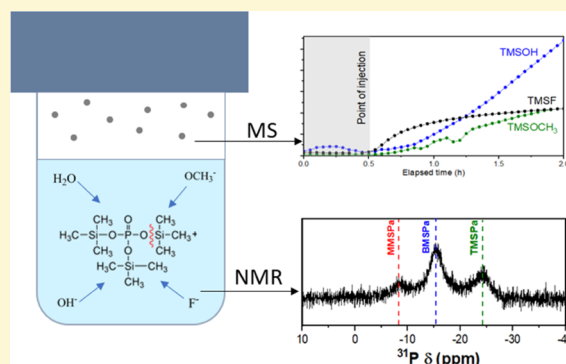
O rganic carbonate-based Li-ion battery electrolytes are state of the art because of their superior combination of performance metrics, such as high ionic conductivity, low viscosity, and thermal stability over a wide temperature range.[1] These electrolytes are also known for their ability to form electrode-passivating layers on the negative Li-ion graphite electrode, commonly termed solid electrolyte interphases (SEIs), which are necessary to stabilize the electrode/electrolyte interfaces and prevent cell failure. When the graphite electrode potential is pushed sufficiently negative ($\lesssim 1$ V vs Li^+/Li), the organic carbonate solvent reductively decomposes, forming products of which Lewis bases (LBs) (e.g., RO^-, $C_2O_4^{2-}$, RCO_3^{2-}, etc.) are the most notable. Depending on their respective solubility, these Lewis bases may combine with Li^+ and precipitate on the electrode in form of an electrically insulating yet Li^+-conductive SEI.[2,3] Ethylene carbonate (EC) is the archetype Li-ion electrolyte solvent and is known to decompose into both organic and inorganic compounds like lithium alkyl carbonates, alkoxides, oxalates, and various other lithium salts.[1] Lithium hexafluorophosphate ($LiPF_6$), similarly being the archetype electrolyte salt, normally decomposes to form fluorides (e.g., lithium or hydrogen fluoride (LiF/HF)) and phosphorus-containing compounds. Regardless of the species formed, only a few of the products contribute to the effective SEI while the rest simply lead to loss of active lithium and higher cell impedance.[4] Possibly worse,

some of the formed products could even further propagate unwanted side reactions and accelerate the failure of the cell.[5]

Electrolyte additives are typically functional molecules dissolved at low concentrations (<5 wt %) in the electrolyte to optimize their physicochemical properties. Examples are SEI formers (e.g., vinylene carbonate), flame retardants (e.g., hexamethoxycyclophosphazene (HMPN) and trimethyl phosphate (TMP)), cathode surface layer formers (e.g., *n*-butylferrocene), etc.[1] A large group of performance-enhancing additives contains organosilicon silyl groups (R_3Si), which when included are known to react with HF, a harmful molecule often encountered in operating Li-ion cells. Particularly, the silyl-functionalized phosphites ($P(OR)_3$) and phosphates ($O=P(OR)_3$) have been researched for years.[6−10] One well-known representative is tris-(trimethylsilyl)phosphate (TMSPa), which, apart from scavenging HF, has also been claimed to be "multifunctional", e.g., in the sense of being an electrode layer former (both on the positive and negative
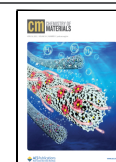
electrodes).[11,12] Indeed, the group of Jeff Dahn and others showed that $LiNi_{1/3}Mn_{1/3}Co_{1/3}O_2$(NMC)/graphite-based Li-ion cells with TMSPa added display longer cycle and calendar life and exhibit lower impedance.[13,14] Bolli et al. showed that TMSPa used as an additive in Li-rich NMC/graphite cells does not necessarily form a SEI or CEI by being electrochemically reduced/oxidized, but by also scavenging other fluorides, such as LiF residues, lowers the cell impedance.[11] Removing the highly resistive LiF from the SEI while replacing it with side products from TMSPa degradation, such as P- and O-rich compounds, would increase Li^+ conductivity while at the same time suppress adverse side reactions within the cell.[15]

Previous studies from our group and others also indicated that TMSPa may not only remove fluorides but could also react with oxide-based impurities,[14,16,17] such as hydroxides. Experimental evidence was, however, merely based on the observation of reduced extent of CO_2 evolution (presumed to derive from the OH^--catalyzed EC ring opening described in reactions 1 and 2) within Li-ion cells containing TMSPa, and no further support for a specific reaction mechanism was provided.[14] In principle, all Lewis bases could initiate a nucleophilic attack on the carbonyl carbon of EC and thereby trigger a ring-opening reaction and release of CO_2

$$\text{(1)}$$

$$\text{(2)}$$
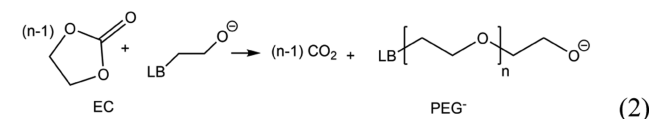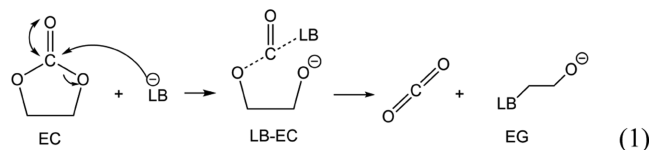
Degradation of EC at elevated temperatures, initiated by Lewis bases, leads to the formation of poly(ethylene glycol) (PEG)-like polymers,[18] which either deposit on the active materials or dissolve in the electrolyte with increased cell impedance as a result.[5] Moreover, this process is accompanied by an evolution of CO_2, which, in turn, could be scavenged by remaining Lewis bases to form a range of carbonates,[19,20] formates,[21] etc.

$$\text{(3)}$$
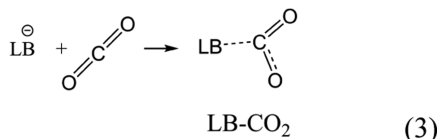
Basic OH^- reacting with CO_2 forming inorganic carbonates would be the most prominent example thereof. These thermally activated processes are competing and highly complex with the involvement of several different Lewis bases, as reflected by the richness of various species typically found in the SEI. If these Lewis bases remain active after the essential SEI is formed, the SEI will continue to grow, increase impedance, and shorten the lifetime of the cell.

Three of the most commonly reported Lewis bases formed in the Li-ion cell are F^-, OH^-, and $^-OCH_3$. F^- is formed as a result of decomposition of fluorinated salts (like $LiPF_6$) and additives (e.g., fluoroethylene carbonate (FEC)). LiF is practically insoluble in the solvents and hence precipitates on the electrode surfaces whenever formed. OH^-, on the other hand, is typically formed from the reduction of trace water in the electrolyte.[22] Hydroxides may also result from the reaction of Li_2O with water.[23] LiOH is predicted to be more soluble

than LiF in conventionally used solvents. $^-OCH_3$ may form as a result of electrochemical reduction of semicarbonates like diethylene carbonate (DEC). The solubility of $LiOCH_3$ is predicted to lie in between LiF and LiOH.[24]

The aim of this study is to investigate the reactivity of the silyl group, as included in TMSPa, towards Lewis bases typically formed in Li-ion cells, such as F^-, OH^-, and $^-OCH_3$. We hypothesize that a significant beneficial action of silyl-functionalized electrolyte additives derives from their general ability to scavenge Lewis bases and thereby suppress electrolyte decomposition and cell impedance growth associated with the above reactions 1−3. An elucidation of the underlying reaction mechanisms of silyl-group-functionalized electrolyte additives promises to unlock a deeper understanding of Li-ion chemistry and lead the way to further optimization of the degradation products formed within the battery cells.

■ EXPERIMENTAL SECTION

Battery-grade EC (Sigma-Aldrich) and DEC (Sigma-Aldrich) were introduced into the glovebox as received from the suppliers. DEC was dried with molecular sieves and then mixed with EC (which was heated up to 50 °C to melt). The mixture of EC/DEC used in this study is in a 1:1 volume ratio, unless otherwise stated. The solvent mixture was further dried with molecular sieves. The water content is around 10 ppm as tested by the Karl Fisher method. LiF (Alfa Aesar, 99.85%), LiOH (Alfa Aesar, 99.85%), and $LiOCH_3$ (Sigma-Aldrich, 98%) were dried at 120 °C in a Büchi oven overnight under vacuum inside the glovebox. Saturated Lewis base solutions were prepared by adding 100 mg of Lewis bases in 2 mL of EC/DEC mixture in separate vials. The vials were sealed and allowed to stir in a magnetic stirrer at least overnight before performing any test. This procedure was performed to make sure that a saturated Lewis base solution is taken as a starting sample. TMSPa, hydroxy-trimethylsilane (TMSOH), and methoxy-trimethylsilane ($TMSOCH_3$) from Sigma-Aldrich (≥98, 97.5, and 99% respectively) were used as received from suppliers.

Nuclear Magnetic Resonance. For NMR, a JEOL (^{1}H, 500 MHz; ^{31}P, 162 MHz; ^{19}F, 376 MHz) spectrometer was used, and chemical shifts were recorded in parts per million. Anhydrous dimethylsulfoxide (DMSO)-d_6 (99.9%) from VWR was further dried with molecular sieves and was used as a deuterated solvent. Plastic falcon tubes for electrolyte storage and fluorinated ethylene propylene (FEP) NMR tube liners (outer diameter: 5 mm, Wilmad-LabGlass) were used. They were used as a precautionary measure to avoid any reaction between glass and fluorides. The mouth of the FEP tube was closed with poly(tetrafluoroethylene) (PTFE) plug. For each NMR sample test, 400 μL of DMSO-d_6 was added to 100 μL of sample solution. Then, each FEP NMR tube was placed inside a glass NMR tube (inner diameter: 5 mm), which was again closed with a PTFE stopper. The solution storage and sample preparation were done in the glovebox and the H_2O content inside it was kept below 1 ppm. All spectra were processed and analyzed by MestReNova 6.0.2-5475.

Mass Spectrometry. The gas analysis setup consists of a custom-made injection cell, which is a blue-capped bottle of 10 mL volume (Duran). The lid of the bottle has three connections: (1) an outlet to periodically sample the evolved gases to the mass spectrometer (Pfeiffer PrismaPlus QME220), (2) an inlet to refill the cell with fresh Ar gas, and (3) a syringe for injection. The temperature and pressure in the cell are monitored using a high precision transducer (Keller-Druck). The sampling system and the cell are integrated inside a temperature-controlled incubator chamber (Tritec, Germany). The temperature is set to 30 °C for all of the experiments.[25] LiF, LiOH, and $LiOCH_3$ were grinded in a mortar and pestle for at least 5 min before making the sample solution. To monitor gas evolution, two different sets of samples were prepared with different protocols: (1) 50 mg of Lewis bases and 800 μL of DEC were mixed in the bottom of the vial and 400 μL of EC/DEC was taken in the syringe, and this

mixture is referred to as saturated or unfiltered and (2) 50 mg of Lewis base was mixed with 800 μL of DEC. Then, this mixture was filtered into a reaction vial and 400 μL of EC/DEC was taken in the syringe. This mixture is referred to as filtered. For the experiments with the additive, 5 vol % TMSPa was taken together with 400 μL of EC/DEC in the syringe. The time between each sampling point was set to 180 s, and an initial baseline was performed until there was a stable background signal. Once a stable background is achieved, reactants from the syringe were mixed with the reactants in the vial and periodic sampling was done as stated previously. The solution was magnetically stirred to ensure a homogeneous mixing. The partial pressure of gas species in Ar flow is documented as normalized ion current, with respect to Ar and surface area of the Lewis base powder. Each gas species is recorded at a relevant mass-to-charge ratio (m/z): H$_2$-2, O$_2$-32, Ar-36, CO$_2$-44, TMSPa-73, TMSOH-75, TMSF-77, TMSOCH$_3$-89, and DEC-91. The gas profiles for each experiment were compared with its blank, i.e., EC/DEC mixture only. For the experiments with additives, the gas evolved was compared with additive-added blank samples.

Computational Details. Screening studies using the GFN2-xTB model[26] to compute the free energy of reaction at 298 K have been performed to sample the manifold of structural conformations possible for the reactants and the products at every reaction step in the decomposition of TMSPa. The GFN2-xTB model is generally good at describing geometries and intermolecular bond energies for molecular systems. However, for intramolecular bond energies, semiempirical tight-binding methods are generally not as reliable. Thus, before the screening study, we performed density functional theory (DFT) calculations for the gas-phase reactions using the molecular structures obtained from the xTB geometry optimizations as input to ensure that the semiempirical xTB model accurately captures the correct trends in computed reaction energies (breaking and formation of intramolecular bonds). For this purpose, we used Gaussian09[27] and the B3LYP functional[28−31] with a Dunning correlation consistent basis set (aug-cc-pVDZ). Weak nonlocal interactions (vdW-forces) were accounted for using the Grimme D3 aposteriori vdW correction scheme. All structures were geometry optimized until the forces on each atom were less than 0.00077 eV/Å. While absolute values can be off by a maximum of 0.4 eV for the computed reaction energies, the trends, i.e., signs and magnitudes of the computed reaction energies, were found to be in line with the DFT data; see results in the Supporting Information. In the screening study, we always computed the reaction energies considering all reactants and products in each simulation to also account for the important intermolecular interactions. For example, the TMSPa/H$_2$O reaction was simulated, allowing TMSPa and H$_2$O to interact first, as compared to the comparison above for the intramolecular reaction energies, where each molecule was treated separately in the calculation. To obtain reliable reaction energies, we further tested the effect the environment has on the reaction energies by considering three different cases: (i) gas phase, (ii) using an implicit solvation model, namely, the polarizable continuum model (PCM), and (iii) the inclusion of effects from explicit solvation by adding EC to satisfy the possibilities to form hydrogen bonds. After a thorough testing procedure, we found that accounting for the possible formation of molecular complexes with reactants and products has the largest effect and is necessary to obtain reaction energies that support the experimental observations. Therefore, all reaction energies reported were modeled keeping all reaction products along the reaction chain. For a complete discussion of the validity of the theoretical calculations and for figures showing the structural models used, we refer to the Supporting Information.

RESULTS AND DISCUSSION

NMR spectra for the reaction medium (EC/DEC), the individual reactants (TMSPa and Lewis bases) dissolved in EC/DEC, and anticipated products were first acquired, as shown in Figure 1, before the reactivity of the silyl group toward the LBs was investigated. Most relevant peaks are
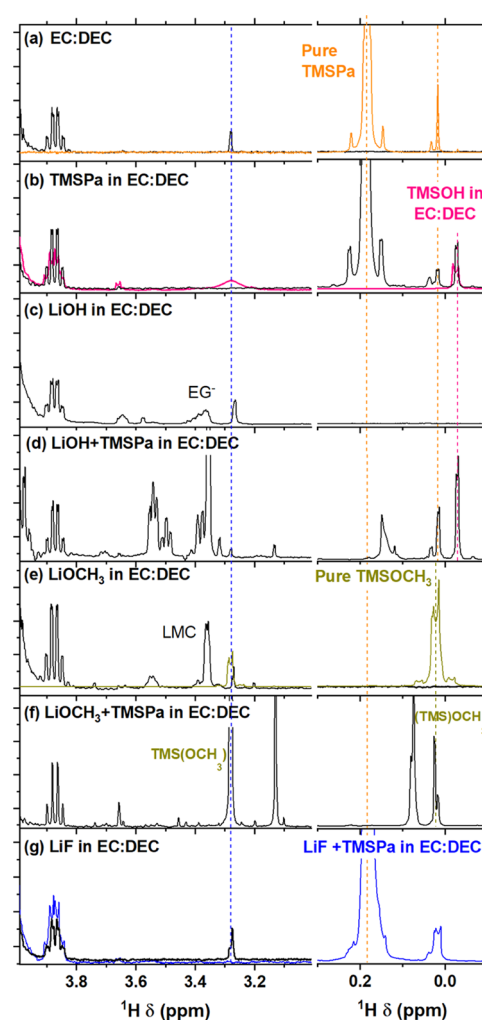

Figure 1. ^{1}H liquid NMR spectra of (a) EC/DEC, orange: pure TMSPa, (b) TMSPa in EC/DEC, pink: TMSOH in EC/DEC, (c) LiOH mixed in EC/DEC, (d) LiOH mixed in EC/DEC with TMSPa, (e) LiOCH$_3$ mixed in EC/DEC, olive green: pure TMSOCH$_3$, (f) LiOCH$_3$ mixed in EC/DEC with TMSPa, and (g) LiF mixed in EC/DEC, blue: LiF mixed in EC/DEC with TMSPa.

observed in the 3−4 δ (ppm) and −0.1−0.3 δ (ppm) range (see the Supporting Information for full spectral ranges recorded (Figure S1)). For the EC/DEC solution, well-known satellite peaks assigned to DEC are visible for ∼3.9 ppm and are included as a reference here. H$_2$O trace impurities are still present in the mixture and identified as a singlet at 3.28 ppm in ^{1}H NMR. Indeed, Karl Fischer titration showed that the solvent mixture contains a few tens of ppm of water as impurities, thus indicating that the protonated species observed at a chemical shift in the range 3−4 ppm could be detected with high sensitivity. TMSPa displays a main set of peaks at ∼0.18 ppm assigned to its methyl −CH$_3$ groups, whereas minor yet detectable peaks at 0.03 ppm assigned to an unknown impurity in the TMSPa additive solution are identified (Figure 1a, orange). Interestingly, when TMSPa is added to the EC/DEC solution, the peak assigned to water vanishes (Figure 1b, black), while a new peak at −0.02 ppm appears. The latter peak is assigned to TMSOH, a proposed product of the reaction

$$\text{TMSPa} \quad\quad \text{LB} \quad\quad \text{TMS-LB} \quad\quad \text{BMSPa-H/Li} \qquad (4)$$
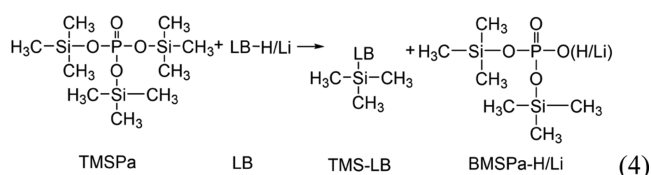
(where LB is the OH^-) confirmed by the reference TMSOH spectrum (Figure 1b, pink). BMSPa stands for bis-(trimethylsilyl)phosphate, represents TMSPa that lost 1 trimethylsilyl (TMS) unit, and is also believed to be observed as a minor peak at −15 ppm by ^{31}P NMR (Figure 2a, black).
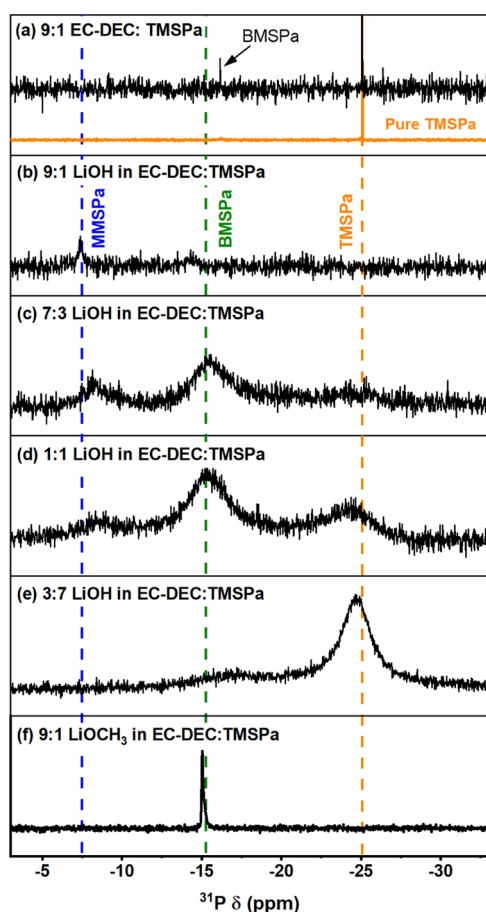

Figure 2. ^{31}P liquid NMR spectra showing the formation of the intermediates upon the reaction of LiOH and TMSPa in the presence of solvents. The broadening of the ^{31}P spectral lines is associated with scalar hydrogen coupling.[36]

Interestingly, in our initial simulations of hydrolysis of TMSPa according to reaction 4, the energy of reaction $\Delta E > 0$. Thus, in the gas phase, the reaction is found to be endothermic (cf. Table S1 in the Supporting Information). Allowing for intermolecular interactions for both reactants and products, together with the addition of explicit solvent molecules (EC), lowers ΔE and makes the reaction exothermic and spontaneous. In this case, a molecular complex between BMSPa and the additional EC is formed, cf. reaction routes illustrated in Figure S2 in the Supporting Information. These results suggest that the ability of the reaction product to form energetically favorable intermolecular interactions (primarily hydrogen bonding) is important for an efficient breakage of the TMSPa's O—Si bond. The resulting lowest energies of reaction

from the GFN2-xTB calculations of the first step of TMSPa/H_2O reaction (Figure 3) show that the hydrolysis of TMSPa is
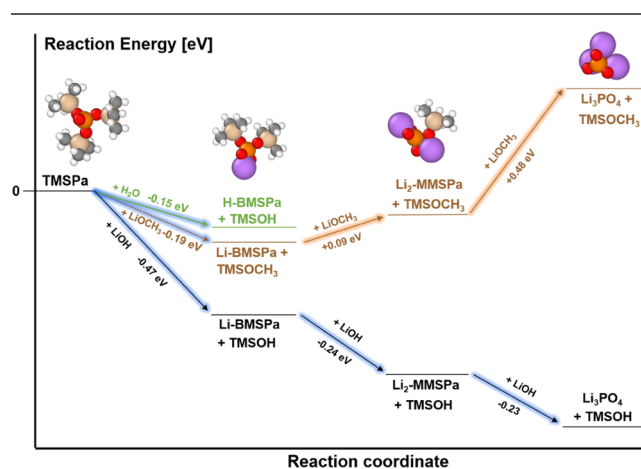

Figure 3. Lowest energy of reaction vs reaction coordinate found in GFN2-xTB screening for the TMSPa/H_2O, TMSPa/LiOH, and TMSPa/OCH_3 reactions. For the TMSPa/H_2O reaction, only the first step is shown. In the modeling, we explicitly account for the intermolecular interactions between reactants and reaction products. In the case of H_2O, an explicit EC molecule is added to ensure that all hydrogen bonds are accounted for (cf. Supporting Information).

slightly exothermic. Results presented thus far evidence that TMSPa does react with neither EC nor DEC but rather with H_2O, which is desired from a practical perspective, to remove residual water from a Li-ion battery electrolyte. After establishing this baseline, the reactivity of three lithiated Lewis bases typically found in the SEI, namely, LiOH, $LiOCH_3$, and LiF toward TMSPa was investigated.

LiOH. Adding LiOH to EC/DEC results in the formation of new compound(s) as evidenced from the appearance of new peaks at 3.36, 3.53, and 3.61 ppm (Figure 1c). The peak at 3.36 ppm is assigned to a $-[CH_2-CH_2-O]-$ fragment of ethylene glycol (EG^-), which is likely derived from LB-triggered ring opening of EC by OH^- along with the release of CO_2 according to Reaction 1, as also previously reported.[32] EG^- thus formed may further polymerize EC forming poly(ethylene glycol) (PEG^-) along with additional CO_2 (Reaction 2). Indeed, our group has previously observed increased electrolyte viscosity upon the formation of OH^- during the first few cycles of the Li-ion cell.[33] Further support for such a scenario was found in the form of a continuous evolution of CO_2 gas when EC/DEC contacted LiOH compared to the blank experiment in Figure 4a. In the blank case, only the EC/DEC solution is injected into the reaction vial containing DEC and only CO_2 already dissolved in these solvents escapes to the continuously flushed Ar headspace. When LiOH is present, a part of CO_2 will be scavenged by OH^- forming lithium bicarbonate and eventually Li_2CO_3 (Reaction 3), hence explaining the initially lower CO_2 concentrations in the headspace (Figure 4a).[34] Interestingly, when TMSPa was added to LiOH in a EC/DEC mixture significantly, more CO_2 evolved (Figure 4a) along with the formation of much more PEG, other solvent degradation products, and TMSOH (Figure 1d). Since neither TMSPa nor TMSOH decomposes EC/DEC to any greater extent (Figure 1b, pink), the enhanced EC decomposition rate is related to an increased reactivity of OH^- when TMSPa is present. We hypothesize that TMSPa acts as an anion receptor[35] increasing
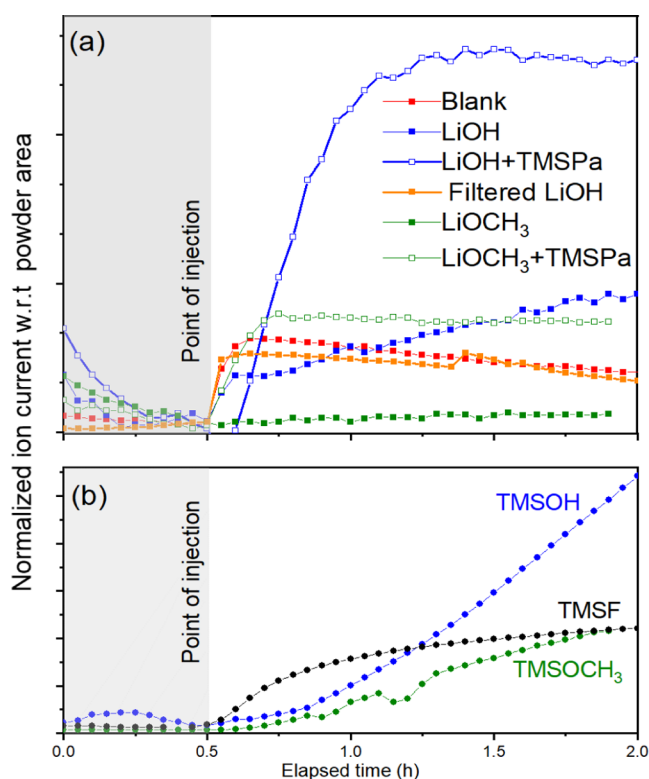
Figure 4. (a) CO_2 gas evolution profile of blank solution and Lewis bases with solvents with and without TMSPa. Gray area represents the region of background baseline. (b) TMS-LB evolution profiles, as recorded from the mass spectrometer.

the dissolution of LiOH, thus dissolving more OH^-, which accelerates the ring opening of EC and the evolution of CO_2. To confirm, the CO_2 evolution was monitored for a filtered LiOH/EC/DEC solution, i.e., thus removing any eventual solid LiOH in EC/DEC when it comes in contact with TMSPa. Upon filtration, there will thus be a limited OH^- concentration and no additional LiOH to be dissolved in the reaction cell due to the presence of TMSPa. A filtered solution clearly shows lower CO_2 evolution, which supports the notion that TMSPa is able to produce free OH^- by solubilizing more LiOH in the unfiltered case, where there is an excess of solid LiOH powder sitting at the bottom of the reaction vial.

In any case, OH^- eventually breaks the O–Si bond in TMSPa to form TMSOH, as evidenced by the relatively strong peak at −0.02 ppm in Figure 1d, and the continuous evolution of gaseous TMSOH (Figure 4b) when TMSPa comes in contact with LiOH. More importantly, TMSPa was largely consumed in the LiOH-saturated EC/DEC solution as evidenced by the nearly complete disappearance of the peak at 0.18 ppm (Figure 1d).

The influence of the TMSPa concentration was therefore more closely examined by mixing saturated LiOH in EC/DEC with TMSPa in 9:1, 7:3, 1:1, and 3:7 volume ratios. Indeed, ^{31}P NMR spectra reveal that the signal from the nearly completely consumed TMSPa (Figure 2b) reappears at higher concentrations (Figure 2c–e). Moreover, two peaks assigned to the intermediate products BMSPa and mono(trimethylsilyl)-phosphate (MMSPa, loss of 2 TMS units from TMSPa), as illustrated in Figure 3, are distinguished. The TMS units attached to the central phosphate group of TMSPa would thus be stepwise consumed until only the final product, Li_3PO_4,

without any TMS units attached remains. The GFN2-xTB calculations show that the reaction between LiOH and TMSPa is exothermic, and we expect that the reaction proceeds until Li_3PO_4 once the reactants meet (Figure 3). These data are in line with the experimental observations of largely consumed MMSPa when LiOH is in excess (Figure 2b). Lithium phosphate does have a low solubility in EC/DEC (hence not detected by our ^{31}P NMR spectrometer, Figure 2b).

LiOCH₃. Another LB typically found in Li-ion cells is methoxide (OCH_3^-), e.g., resulting from the reduction of the linear carbonate solvents.[37] The ^1H NMR of $LiOCH_3$ mixed in EC/DEC (Figure 1e) shows new signals at 3.37 and 3.54 ppm. The peak at 3.37 ppm was first tentatively assigned to 2-methoxyethanolate formed as a result of the OCH_3^--induced EC ring-opening reaction. However, the CO_2 gas profile from MS (Figure 4a) showed otherwise. CO_2 present in the EC/DEC solvent mixture is rather observed to be readily consumed when in contact with $LiOCH_3$ likely to form lithium methyl carbonate (LMC)

$$O=C{\overset{O}{\diagdown}} + Li-OCH_3 \longrightarrow Li^+ \;\; {\overset{O}{\underset{O}{\overset{\|}{-}C-O}}}{-}O-CH_3$$

$$LMC \qquad (5)$$
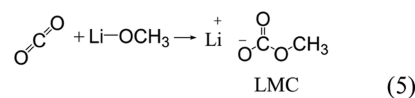
which is an often reported component of the SEI,[38] though with a poor Li^+ conductivity.[39] Based on these results, the new peak at 3.37 ppm appearing in the ^1H NMR spectrum is assigned to LMC instead of methoxyethanolate. $LiOCH_3$ is thus not anticipated to induce EC ring opening, but rather scavenges CO_2, judging from the nearly complete disappearance of CO_2 evolution from the solvents (Figure 4b).

To investigate the reaction between OCH_3^- and TMSPa, ^1H and ^{31}P NMR were performed on a EC/DEC solution in which $LiOCH_3$ is dissolved and to which TMSPa is added (Figures 1f and 2f, respectively). The ^{31}P NMR shows a single and slightly broadened peak at −15.05 ppm assigned to BMSPa. The ^1H NMR also shows peaks belonging to BMSPa along with new peaks at 3.13 and 3.28 ppm assigned to TMSOCH₃. Interestingly, the signal from TMSPa disappears, again demonstrating that the additive is completely consumed. Addition of TMSPa also removed the species appearing at 3.37 ppm, tentatively assigned to LMC. Either TMSPa reacts directly with LMC or indirectly, e.g., favoring the backward direction of reaction 5 by scavenging $LiOCH_3$ according to Le Chatelier's principle. Indeed, the addition of TMSPa to $LiOCH_3$ solution increases the evolution of CO_2, but only to a level comparable to if all CO_2 originally dissolved in the EC/DEC solution would be released (Figure 4a). Evidently, $LiOCH_3$ reacts with TMSPa breaking the molecule at the O–Si bond with TMSOCH₃ and BMSPa as reaction products. Upon a direct comparison with the ^1H NMR spectrum of pure TMSOCH₃ (Figure 1e), the chemical shifts and integrals of the peaks at 0.02 and 3.28 ppm were found to fit very well with the −OCH₃ and −TMS groups of pure TMSOCH₃, respectively. Moreover, the reaction product TMSOCH₃ was clearly detected by MS when TMSPa came in contact with $LiOCH_3$ and continued to evolve throughout the experiment (Figure 4b). Interestingly, only the peak at −15.05 ppm in ^{31}P NMR and 0.07 ppm in ^1H NMR attributed to the BMSPa moiety is identified. The reaction between TMSPa and $LiOCH_3$ apparently stops at BMSPa and does not proceed to MMSPa and hence likely not to Li_3PO_4 either. Indeed, in the GFN2-xTB calculations for the TMSPa/LiOCH₃ reaction, a minimum in the reaction energy with respect to the reaction

coordinate is found for BMSPa, cf. Figure 3. The LiBMSPa product side is found at a higher energy than anticipated from the calculated gas-phase reactions due to the formation of a molecular complex with the reaction product. Hence, accounting for explicit interactions is important given that the gas-phase reactions with and without the addition of an implicit solvent description are strongly exothermic (see Table S1 in the Supporting Information). In a continuous reaction chain, these stabilizations are even larger, making LiBMSPa/LiOCH$_3$ and Li$_2$MMSPa/LiOCH$_3$ endothermic. The most stable configurations found with the GFN2-xTB method are shown in Figure S5 in the Supporting Information.

LiF. The reactivity of silyl groups towards fluorides has already been investigated extensively, also as included in TMSPa.[14,40] LiF is practically insoluble in EC/DEC, and we confirm that adding LiF to EC/DEC resulted in no signs of new products, neither in ^{1}H NMR (Figure 1g) nor ^{19}F NMR within the timescale of the experiment. When TMSPa was added to LiF in EC/DEC mixture, no new species appeared in the ^{1}H NMR spectrum (Figure 1g), but in the ^{19}F NMR spectrum, a characteristic peak at −154.71 ppm was observed, which was attributed to TMSF (see Figure S1 in the Supporting Information). Indeed, the gas analysis also confirmed previous observations of TMSPa reacting spontaneously with LiF to yield TMSF analogously to Reaction 4 in which F$^-$ breaks the Si−O bond of TMSPa and combines with the TMS moiety. The dissolved TMSF is volatile as observed by the MS headspace analysis (Figure 4b).[12,41] Since these observations merely confirm both experimental and theoretical observations and the conclusion made previously, we do not proceed with further analysis. We do however highlight that F$^-$ displays the same expected reaction as for OH$^-$ and $^-$OCH$_3$ toward TMSPa, thus demonstrating that the reactivity of the silyl groups is not specific toward fluorides but may scavenge several Lewis bases generally found in Li-ion cells.

SUMMARY AND CONCLUSIONS

Silyl groups are important functional components in a wide range of molecular electrolyte additives developed to enhance the performance of state-of-the-art Li-ion batteries. Focus herein is on a well-known representative thereof, trimethylsilylphosphate, which connects three silyl groups to a central phosphate. Our hypothesis that the silyl groups not only specifically react with fluorides, as already widely reported, but also generally react with Lewis bases is confirmed. Water (H$_2$O), hydroxide (OH$^-$), and methoxide ($^-$OCH$_3$) are here brought forward as candidates well representing three types of Lewis bases found in Li-ion cells. ^{1}H, ^{19}F, and ^{31}P-nuclear magnetic resonance combined with headspace gas analysis are applied to monitor TMSPa, the Lewis base, as well as both soluble and volatile reaction products. Theoretical simulations have been performed, which provide support for the experimental observations. On the basis of our findings, we conclude that silyl-group-functionalized molecular additives are beneficial because of their ability to scavenge a range of potentially harmful Lewis bases in the Li-ion cell. Lewis bases are here confirmed to ring-open the electrolyte solvent ethylene carbonate (EC) to release CO$_2$ and ethylene glycols (Reaction 1). The latter degradation product further polymerizes and increases ionic resistance of the electrolyte (Reaction 2).[5] CO$_2$ may be scavenged to form resistive electrode deposits (Reaction 3), such as LMC (Reaction 5). Including silyl-group-based additives in the electrolyte may hence effectively

eliminate such adverse effects immediately upon cell assembly by removing Lewis bases and break the autocatalytic electrolyte decomposition cycle of the solvent (combining Reactions 1 and 2). Later on, upon cycling, silyl groups can dissolve and replace highly resistive deposits of the graphite SEI, be it LMC or LiF, with the more ionically conducting Li$_3$PO$_4$.[42] In addition, removal of Lewis bases, such as H$_2$O, is also known to have a beneficial influence on the stability of the commonly employed LiPF$_6$ electrolyte salt.[43] These findings explain why Li-ion cells with silyl-group-based additives display lower impedance and longer cycle life. Although the fate of the resulting TMS-LB species is not further investigated here, these species are soluble in the electrolyte and may not necessarily further react to form resistive deposits and/or induce active lithium loss in the cell. Intermolecular interaction between TMSPa, Lewis bases, and the products is found to be necessary to explain the reaction mechanisms. Gas-phase reaction energies, treating only reactants and products explicitly, are found not sufficient to account for the hypothesized and experimentally proven behavior. This is particularly seen in the cases where there are products offering the formation of new hydrogen bonds, such as the TMSPa/H$_2$O and TMSPa/LiOH reactions. Intermolecular physicochemical effects, such as anion reception, ionic complex formation, and hydrogen bonding, are found more important than expected but remain a subject of future studies. Model studies combining experiments and simulations, as presented herein, are essential to provide the building blocks necessary to establish a deeper fundamental understanding of the Li-ion cell chemistry and the highly complex reaction mechanisms found therein.

■ ASSOCIATED CONTENT

ⓢ Supporting Information

The Supporting Information is available free of charge at https://pubs.acs.org/doi/10.1021/acs.chemmater.2c00345.

^{1}H, ^{19}F NMR spectra, and computational details etc (PDF)

■ AUTHOR INFORMATION

Corresponding Authors

Neeha Gogoi − *Department of Chemistry, Ångström Laboratory, Uppsala University, SE-751 21 Uppsala, Sweden;* ⓞ orcid.org/0000-0002-0481-5544; Email: neeha.gogoi@kemi.uu.se

Erik J. Berg − *Department of Chemistry, Ångström Laboratory, Uppsala University, SE-751 21 Uppsala, Sweden;* ⓞ orcid.org/0000-0001-5653-0383; Email: erik.berg@kemi.uu.se

Authors

Erik Bowall − *Department of Chemistry, Ångström Laboratory, Uppsala University, SE-751 21 Uppsala, Sweden*

Robin Lundström − *Department of Chemistry, Ångström Laboratory, Uppsala University, SE-751 21 Uppsala, Sweden;* ⓞ orcid.org/0000-0001-9070-9264

Nataliia Mozzhukhina − *Department of Chemistry, Ångström Laboratory, Uppsala University, SE-751 21 Uppsala, Sweden;* Present Address: Department of Physics, Chalmers University of Technology, SE 412 96 Göteborg, Sweden; ⓞ orcid.org/0000-0001-6798-9704

Guiomar Hernández − *Department of Chemistry, Ångström Laboratory, Uppsala University, SE-751 21 Uppsala, Sweden;* ⊙ orcid.org/0000-0002-2004-5869

Peter Broqvist − *Department of Chemistry, Ångström Laboratory, Uppsala University, SE-751 21 Uppsala, Sweden;* ⊙ orcid.org/0000-0002-9842-4332

Complete contact information is available at:
https://pubs.acs.org/10.1021/acs.chemmater.2c00345

Notes

The authors declare no competing financial interest.

■ REFERENCES

(1) Xu, K. Nonaqueous Liquid Electrolytes for Lithium-Based Rechargeable Batteries. *Chem. Rev.* **2004**, *104*, 4303−4418.

(2) Wilken, S.; Treskow, M.; Scheers, J.; Johansson, P.; Jacobsson, P. Initial Stages of Thermal Decomposition of LiPF6-Based Lithium Ion Battery Electrolytes by Detailed Raman and NMR Spectroscopy. *RSC Adv.* **2013**, *3*, 16359−16364.

(3) Shi, F.; Zhao, H.; Liu, G.; Ross, P. N.; Somorjai, G. A.; Komvopoulos, K. Identification of Diethyl 2,5-Dioxahexane Dicarboxylate and Polyethylene Carbonate as Decomposition Products of Ethylene Carbonate Based Electrolytes by Fourier Transform Infrared Spectroscopy. *J. Phys. Chem. C* **2014**, *118*, 14732−14738.

(4) Heiskanen, S. K.; Kim, J.; Lucht, B. L. Generation and Evolution of the Solid Electrolyte Interphase of Lithium-Ion Batteries. *Joule* **2019**, *3*, 2322−2333.

(5) Kitz, P. G.; Novák, P.; Berg, E. J. Influence of Water Contamination on the SEI Formation in Li-Ion Cells: An Operando EQCM-D Study. *ACS Appl. Mater. Interfaces* **2020**, *12*, 15934−15942.

(6) Tarnopolsky, V. Electrolyte for rechargeable lithium battery, and rechargeable lithium battery including same. U.S. Patent US7494746B22009.

(7) Mai, S.; Xu, M.; Liao, X.; Hu, J.; Lin, H.; Xing, L.; Liao, Y.; Li, X.; Li, W. Tris(Trimethylsilyl)Phosphite as Electrolyte Additive for High Voltage Layered Lithium Nickel Cobalt Manganese Oxide Cathode of Lithium Ion Battery. *Electrochim. Acta* **2014**, *147*, 565−571.

(8) Song, Y. M.; Han, J. G.; Park, S.; Lee, K. T.; Choi, N. S. A Multifunctional Phosphite-Containing Electrolyte for 5 V-Class LiNi 0.5Mn1.5O4 Cathodes with Superior Electrochemical Performance. *J. Mater. Chem. A* **2014**, *2*, 9506−9513.

(9) Wang, D. Y.; Dahn, J. R. A High Precision Study of Electrolyte Additive Combinations Containing Vinylene Carbonate, Ethylene Sulfate, Tris(Trimethylsilyl) Phosphate and Tris(Trimethylsilyl) Phosphite in Li[Ni 1/3 Mn 1/3 Co 1/3]O 2 /Graphite Pouch Cells. *J. Electrochem. Soc.* **2014**, *161*, A1890−A1897.

(10) Peebles, C.; Sahore, R.; Gilbert, J. A.; Garcia, J. C.; Tornheim, A.; Bareño, J.; Iddir, H.; Liao, C.; Abraham, D. P. Tris(Trimethylsilyl) Phosphite (TMSPi) and Triethyl Phosphite (TEPi) as Electrolyte Additives for Lithium Ion Batteries: Mechanistic Insights into Differences during LiNi 0.5 Mn 0.3 Co 0.2 O 2 -Graphite Full Cell Cycling. *J. Electrochem. Soc.* **2017**, *164*, A1579−A1586.

(11) Bolli, C.; Guéguen, A.; Mendez, M. A.; Berg, E. J. Operando Monitoring of F - Formation in Lithium Ion Batteries. *Chem. Mater.* **2019**, *31*, 1258−1267.

(12) Qi, X.; Tao, L.; Hahn, H.; Schultz, C.; Gallus, D. R.; Cao, X.; Nowak, S.; Röser, S.; Li, J.; Cekic-Laskovic, I.; Rad, B. R.; Winter, M. Lifetime Limit of Tris(Trimethylsilyl) Phosphite as Electrolyte Additive for High Voltage Lithium Ion Batteries. *RSC Adv.* **2016**, *6*, 38342−38349.

(13) Sinha, N. N.; Burns, J. C.; Dahn, J. R. Comparative Study of Tris(Trimethylsilyl) Phosphate and Tris(Trimethylsilyl) Phosphite as Electrolyte Additives for Li-Ion Cells. *J. Electrochem. Soc.* **2014**, *161*, A1084−A1089.

(14) Guéguen, A.; Bolli, C.; Mendez, M. A.; Berg, E. J. Elucidating the Reactivity of Tris(Trimethylsilyl)Phosphite and Tris-(Trimethylsilyl)Phosphate Additives in Carbonate Electrolytes - A Comparative Online Electrochemical Mass Spectrometry Study. *ACS Appl. Energy Mater.* **2020**, *3*, 290−299.

(15) Kim, J.; Adiraju, V. A. K.; Rodrigo, N.; Hoffmann, J.; Payne, M.; Lucht, B. L. Lithium Bis(Trimethylsilyl) Phosphate as a Novel Bifunctional Additive for High-Voltage LiNi1.5Mn0.5O4/Graphite Lithium-Ion Batteries. *ACS Appl. Mater. Interfaces* **2021**, *13*, 22351−22360.

(16) Kim, D. Y.; Park, H.; Choi, W. I.; Roy, B.; Seo, J.; Park, I.; Kim, J. H.; Park, J. H.; Kang, Y. S.; Koh, M. Ab Initio Study of the Operating Mechanisms of Tris(Trimethylsilyl) Phosphite as a Multifunctional Additive for Li-Ion Batteries. *J. Power Sources* **2017**, *355*, 154−163.

(17) Mai, S.; Xu, M.; Liao, X.; Xing, L.; Li, W. Improving Cyclic Stability of Lithium Nickel Manganese Oxide Cathode at Elevated Temperature by Using Dimethyl Phenylphosphonite as Electrolyte Additive. *J. Power Sources* **2015**, *273*, 816−822.

(18) Metzger, M.; Strehle, B.; Solchenbach, S.; Gasteiger, H. A. Hydrolysis of Ethylene Carbonate with Water and Hydroxide under Battery Operating Conditions. *J. Electrochem. Soc.* **2016**, *163*, A1219−A1225.

(19) Peng, Z.; Merz, K. M., Jr. Theoretical Investigation of the CO2 + OH- — > HCO3- Reaction in the Gas and Aqueous Phases. **1993**, *115*, 9640 9647. DOI: 10.1021/ja00074a032.

(20) Zhuang, G. V.; Yang, H.; Ross, P. N.; Xu, K.; Jow, T. R. Lithium Methyl Carbonate as a Reaction Product of Metallic Lithium and Dimethyl Carbonate. *Electrochem. Solid-State Lett.* **2006**, *9*, A64−A68.

(21) McMahon, T. B.; Northcott, C. J. The Fluoroformate Ion, FCO 2 −. An Ion Cyclotron Resonance Study of the Gas Phase Lewis Acidity of Carbon Dioxide and Related Isoelectronic Species. *Can. J. Chem.* **1978**, *56*, 1069−1074.

(22) Aurbach, D.; Daroux, M. L.; Faguy, P. W.; Yeager, E. Identification of Surface Films Formed on Lithium in Propylene Carbonate Solutions. *J. Electrochem. Soc.* **1987**, *134*, 1611−1620.

(23) Zhuang, G. V.; Ross, P. N. Analysis of the Chemical Composition of the Passive Film on Li-Ion Battery Anodes Using Attentuated Total Reflection Infrared Spectroscopy. *Electrochem. Solid-State Lett.* **2003**, *6*, No. A136.

(24) Tasaki, K.; Harris, S. J. Computational Study on the Solubility of Lithium Salts Formed on Lithium Ion Battery Negative Electrode in Organic Solvents. *J. Phys. Chem. C* **2010**, *114*, 8076−8083.

(25) Lundström, R.; Berg, E. J. Design and Validation of an Online Partial and Total Pressure Measurement System for Li-Ion Cells. *J. Power Sources* **2021**, *485*, No. 229347.

(26) Bannwarth, C.; Ehlert, S.; Grimme, S. GFN2-XTB - An Accurate and Broadly Parametrized Self-Consistent Tight-Binding Quantum Chemical Method with Multipole Electrostatics and Density-Dependent Dispersion Contributions. *J. Chem. Theory Comput.* **2019**, *15*, 1652−1671.

(27) Frisch, M. J.; Trucks, G. W.; Schlegel, H. B.; Scuseria, G. E.; Robb, M. A.; Cheeseman, J. R.; Scalmani, G.; Barone, V.; Mennucci, B.; Petersson, G. A.; Nakatsuji, H.; Caricato, M.; Li, X.; Hratchian, H. P.; Izmaylov, A. F.; Bloino, J.; Zheng, G.; Sonnenberg, J. L.; Had, M.; Fox, D. J. et al.*Gaussian 09 Citation*;Gaussian, Inc.: Wallingford CT, 2016.

(28) Becke, A. D. Density-Functional Thermochemistry. III. The Role of Exact Exchange. *J. Chem. Phys.* **1993**, *98*, 5648−5652.

(29) Lee, C.; Yang, W.; Parr, R. G. Development of the Colic-Salvetti Correlation-Energy into a Functional of the Electron Density Formula. *Phys. Rev. B* **1988**, *37*, 785−789.

(30) Vosko, S. H.; Wilk, L.; Nusair, M. Accurate Spin-Dependent Electron Liquid Correlation Energies for Local Spin Density Calculations: A Critical Analysis. *Can. J. Phys.* **1980**, *58*, 1200−1211.

(31) Stephens, P. J.; Devlin, F. J.; Chabalowski, C. F.; Frisch, M. J. Ab Initio Calculation of Vibrational Absorption and Circular Dichroism Spectra Using Density Functional Force Fields. *J. Phys. Chem. A* **1994**, *98*, 11623−11627.

(32) Aurbach, D. *Nonaqueous Electrochemistry*; Marcel Dekker, Inc., 1999.

(33) Kitz, P. G.; Lacey, M. J.; Novák, P.; Berg, E. J. Operando Investigation of the Solid Electrolyte Interphase Mechanical and Transport Properties Formed from Vinylene Carbonate and Fluoroethylene Carbonate. *J. Power Sources* **2020**, *477*, No. 228567.

(34) Mozhzhukhina, N.; Flores, E.; Lundström, R.; Nystrom, V.; Kitz, P. G.; Edström, K.; Berg, E. J. Direct Operando Observation of Double Layer Charging and Early SEI Formation in Li-Ion Battery Electrolytes. *J. Phys. Chem. Lett.* **2020**, *11*, 4119−4123.

(35) Qin, Y.; Chen, Z.; Lee, H. S.; Yang, X. Q.; Amine, K. Effect of Anion Receptor Additives on Electrochemical Performance of Lithium-Ion Batteries. *J. Phys. Chem. C* **2010**, *114*, 15202−15206.

(36) Lindon, J. C.; Tranter, G. E.; Holmes, J. L. *Encyclopedia of Spectroscopy and Spectrometry*; Elsevier, 2000.

(37) Xu, K.; Zhuang, G. V.; Allen, J. L.; Lee, U.; Zhang, S. S.; Ross, P. N.; Jow, T. R. Syntheses and Characterization of Lithium Alkyl Mono- and Bicarbonates as Components of Surface Films in Li-Ion Batteries. *J. Phys. Chem. B* **2006**, *110*, 7708−7719.

(38) Parimalam, B. S.; MacIntosh, A. D.; Kadam, R.; Lucht, B. L. Decomposition Reactions of Anode Solid Electrolyte Interphase (SEI) Components with LiPF6. *J. Phys. Chem. C* **2017**, *121*, 22733−22738.

(39) Zhuang, G. V.; Yang, H.; Ross, P. N.; Xu, K.; Jow, T. R. Lithium Methyl Carbonate as a Reaction Product of Metallic Lithium and Dimethyl Carbonate. *Electrochem. Solid-State Lett.* **2006**, *9*, A64−A68.

(40) Bolli, C.; Guéguen, A.; Mendez, M. A.; Berg, E. J. Operando Monitoring of F - Formation in Lithium Ion Batteries. *Chem. Mater.* **2019**, *31*, 1258−1267.

(41) Myers, E. L.; Butts, C. P.; Aggarwal, V. K. BF3·OEt2 and TMSOTf: A Synergistic Combination of Lewis Acids. *Chem. Commun.* **2006**, 4434−4436.

(42) Banerjee, A.; Wang, X.; Fang, C.; Wu, E. A.; Meng, Y. S. Interfaces and Interphases in All-Solid-State Batteries with Inorganic Solid Electrolytes. *Chem. Rev.* **2020**, *120*, 6878−6933.

(43) Xu, K.; Zhang, S.; Jow, T. R.; Xu, W.; Angell, C. A. LiBOB as Salt for Lithium-Ion Batteries:A Possible Solution for High Temperature Operation. *Electrochem. Solid-State Lett.* **2002**, *5*, No. A26.

📖 Recommended by ACS